ARMY RESEARCH LABORATORY

Bio-Mimetic Millimeter-Scale Flapping Wings for Micro Air Vehicles

by Christopher Kroninger, Jeffrey Pulskamp, Jessica Bronson, Ronald G. Polcawich, and Eric Wetzel

ARL-TR-4729 **March 2009**

NOTICES

Disclaimers

The findings in this report are not to be construed as an official Department of the Army position unless so designated by other authorized documents.

Citation of manufacturer's or trade names does not constitute an official endorsement or approval of the use thereof.

Destroy this report when it is no longer needed. Do not return it to the originator.

Army Research Laboratory
Aberdeen Proving Ground, MD 21005-5066

ARL-TR-4729 **March 2009**

Bio-Mimetic Millimeter-Scale Flapping Wings for Micro Air Vehicles

Christopher Kroninger
Vehicle and Technology Directorate, ARL

Jeffrey Pulskamp, Jessica Bronson, and Ronald G. Polcawich
Sensors and Electron Devices Directorate, ARL

Eric Wetzel
Weapons and Materials Research Directorate, ARL

REPORT DOCUMENTATION PAGE	Form Approved OMB No. 0704-0188

1. REPORT DATE *(DD-MM-YYYY)*	2. REPORT TYPE	3. DATES COVERED (From - To)
March 2009	Final	October 2007–October 2008

4. TITLE AND SUBTITLE
Bio-Mimetic Millimeter-Scale Flapping Wings for Micro Air Vehicles

5a. CONTRACT NUMBER

5b. GRANT NUMBER

5c. PROGRAM ELEMENT NUMBER

6. AUTHOR(S)
Christopher Kroninger, Jeffrey Pulskamp, Jessica Bronson Ronald G. Polcawich, and Eric Wetzel

5d. PROJECT NUMBER
1L162618AH80

5e. TASK NUMBER

5f. WORK UNIT NUMBER

7. PERFORMING ORGANIZATION NAME(S) AND ADDRESS(ES)
U.S. Army Research Laboratory
ATTN: AMSRD-ARL-VT-UV
Aberdeen Proving Ground, MD 21005-5066

8. PERFORMING ORGANIZATION REPORT NUMBER
ARL-TR-4729

9. SPONSORING/MONITORING AGENCY NAME(S) AND ADDRESS(ES)

10. SPONSOR/MONITOR'S ACRONYM(S)

11. SPONSOR/MONITOR'S REPORT NUMBER(S)

12. DISTRIBUTION/AVAILABILITY STATEMENT
Approved for public release; distribution is unlimited.

13. SUPPLEMENTARY NOTES

14. ABSTRACT
In this report, we present designs of Micro-Electro-Mechanical System (MEMS) fabricated millimeter-scale flapping wings with some characterization of their structural properties and flapping performance. Wings of varied bio-mimetic design, including membrane and ribs-like structures, are flapped at resonance from lead zirconate titanate (PZT) bending actuators at their base. Laser Doppler vibrometer (LDV) measurements and finite element (FE) analysis predictions of the flapping frequencies and mode shapes and the flapping amplitude of the devices demonstrate the feasibility of fabricating wing systems analogous to insects of the same size scale. We also document the design and progress in implementing a photogrammetric setup, which will be employed for kinematic characterization in this ongoing work.

15. SUBJECT TERMS
MEMS, micro air vehicles, robotics, flapping wings

16. SECURITY CLASSIFICATION OF:			17. LIMITATION OF ABSTRACT	18. NUMBER OF PAGES	19a. NAME OF RESPONSIBLE PERSON
a. REPORT	b. ABSTRACT	c. THIS PAGE			Christopher Kroninger
Unclassified	Unclassified	Unclassified	UU	22	19b. TELEPHONE NUMBER (*Include area code*) 410-278-5690

Standard Form 298 (Rev. 8/98)
Prescribed by ANSI Std. Z39.18

Contents

List of Figures

List of Tables

Acknowledgement

We would like to acknowledge the work of Richard Piekarz and Joel Martin of the U.S. Army Research Laboratory (ARL) and Brian Power of General Technical Services for their contributions in the fabrication of the lead zirconate titanate (PZT) actuators and structures. We would also like to acknowledge the work of Aaron Harrington of the University of Maryland for his contributions to the photogrammetry setup made during his summer internship at ARL.

INTENTIONALLY LEFT BLANK.

1. Objective

The objective of the proposed research is to develop millimeter-scale flapping wings, created through a Micro-Electro-Mechanical System (MEMS) process, that produce lift and flight characteristics similar to those of insects in the same size class. Progress towards this objective will include a study of materials, MEMS design and processes, and wing aeromechanics for a prototype legged MEMS architecture already under development.

2. Approach

2.1 Device Designs

Given the complexity of the aeromechanical design problem, the design of this wing system begins with the presumption that the aerodynamic forces required for flight can be produced by mimicking the kinematic patterns and using structures of similar mechanical properties to those of insects. This effort attempts to demonstrate stroke amplitudes and frequencies that are within the range of actual insect characteristics.

The Drosophila fly (a common fruit fly) is an insect that has been well-characterized in the literature and was the primary model for these designs. A purely bio-mimetic design approach for these prototype wing structures dictated the choice of the wing shape. Additional design variables include the wing span and wing composition using materials currently available in the microfabrication facilities at the U.S. Army Research Laboratory (ARL), including thin-film silicon dioxide, silicon nitride, lead zirconate titanate (PZT), and several common evaporated metals (titanium [Ti], gold [Au], platinum [Pt], nickel [Ni], aluminum [Al]). The design seen in figure 1 features three PZT unimorph mechanically coupled actuators at the base of the wing that are used to directly drive the stroke angle. Altering the phase of the drive signal to the individual actuators permits a limited drive capability of the wing pitch. The actuator performance is a strong function of the underlying structural dielectric layer (figure 2). Gold or silicon vein-structures with patterns similar to those found on real insect wings were included in some designs and may be used to decouple the properties of the actuator from the stiffness of the wing. The fabrication process and materials are similar to the process used for PZT radio frequency (RF) MEMS switches (*1*) with an additional backside release etch.

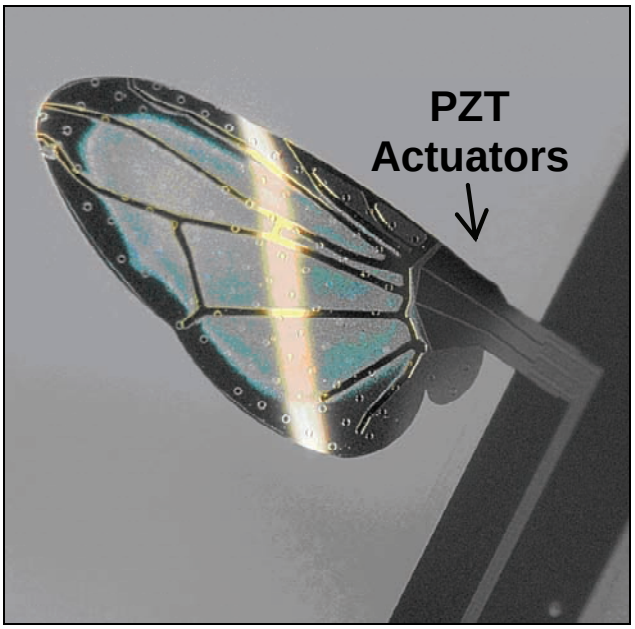

Figure 1. Optical image of a micro-fabricated wing structure (1.5-mm span) with three thin-film PZT actuators at the base of the wing and gold vein-structures deposited on the wing surface.

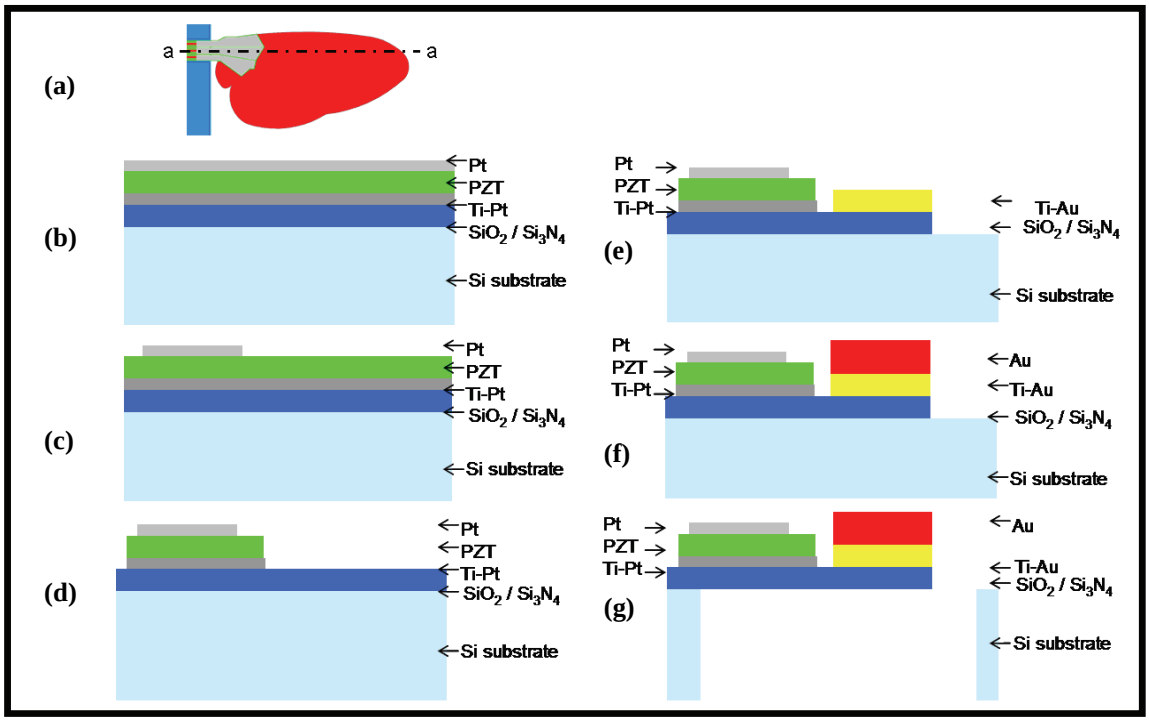

Figure 2. Schematic diagram of fabrication of the wing and actuators (not to scale): (a) top view of a wing and (b–g) process flow.

Figure 2 shows a cross-section view of the micro-wing actuator taken longitudinally along the wing span. Starting with a bare silicon (Si) wafer (figure 2b), a thick composite elastic layer comprised of silicon dioxide and silicon nitride is deposited using plasma enhanced chemical vapor deposition (PECVD). The thickness of this layer was varied from 1 to 3 microns. The film is then annealed at 700 °C in a nitrogen atmosphere. An adhesion/diffusion barrier layer of Ti is sputtered on the PECVD oxide, immediately followed by a sputtered Pt thin-film to serve as the bottom electrode layer of the actuator. The sol-gel PZT is deposited in several layers to achieve the desired thickness of 0.5 micron. The top electrode of Pt is sputter deposited and patterned with argon ion-milling (figure 2c). The PZT for the actuators and the bottom electrode is defined by ion milling (figure 2d). With the PZT actuators patterned, the wing itself is lithographically defined and patterned using a reactive ion etch (RIE) of the composite elastic layer. A thin bi-layer of Ti/Au (200/7300 Å) is deposited and patterned using a liftoff process to provide metal to the bond pads and wing surface (figure 2e). Next, a 2-micron Au layer is deposited via electron beam evaporation and patterned by liftoff (figure 2f). The wing structure is released using a backside deep RIE (DRIE) process that creates a window of free space around the wing (figure 2g). Once the wings are released, the remaining photoresist is removed with an oxygen plasma.

Table 1 summarizes the different combinations of materials and thicknesses used for the wings, including the thickness of the elastic layer as well as the composition of the wing materials, which may include the dielectric PZT layer. Variations of this process flow have been explored and include using silicon-on-insulator (SOI) substrates and using a xenon difluoride (XeF_2) etch to ensure that all the backside Si is removed from the wing structure.

Table 1. Materials and layer thicknesses of the millimeter-scale wings.

Device Design Number	**Elastic Layer (μm)**	**Wing Materials**		
		PZT (0.5 μm)	**Au Full (2 μm)**	**Au V eins**
1	1	x	—	x
2	1	—	x	—
3	1	x	x	—
4	3	—	x	—
5	3	x	—	x
6	3	x	—	—

2.2 Characterization

Characterization of the wing kinematics is performed using several different techniques. A laser Doppler vibrometer (LDV) is used to measure the resonant frequencies and mode shapes of the devices from surface point measurements of the velocity as the wings are excited by a pseudo-random signal. Dynamic angular displacement of the wings excited at resonance is measured by

inspection from long exposure optical images. Finally, measurement of the wing surface displacements is made using a photogrammetric technique that is being developed for this project.

Photogrammetry relies on triangulation from images taken simultaneously from different perspectives to determine the position of a target in space (*2*). The setup seen in figure 3 consists of four 2/3 in. Charge-Coupled Device (CCD) cameras positioned to view the wings from various perspectives. These cameras are controlled with an external trigger coordinated with a strobe light. The strobe light pulse duration is short enough to make the wing appear stationary in the image. As these devices are driven at resonance, the period of the flap stroke is known and any particular location in the flap stroke can be repeatedly imaged by strobing at whole fractions of the drive frequency. In this way, any number of phase-locked images can be acquired and the full wing stroke can be captured by stepping through the period in increments of the desired resolution. This process has been automated to collect all the images when provided a schedule of the three actuator amplitudes and phases as well as the desired number of repeated phase-locked images and resolution of the flap stroke.

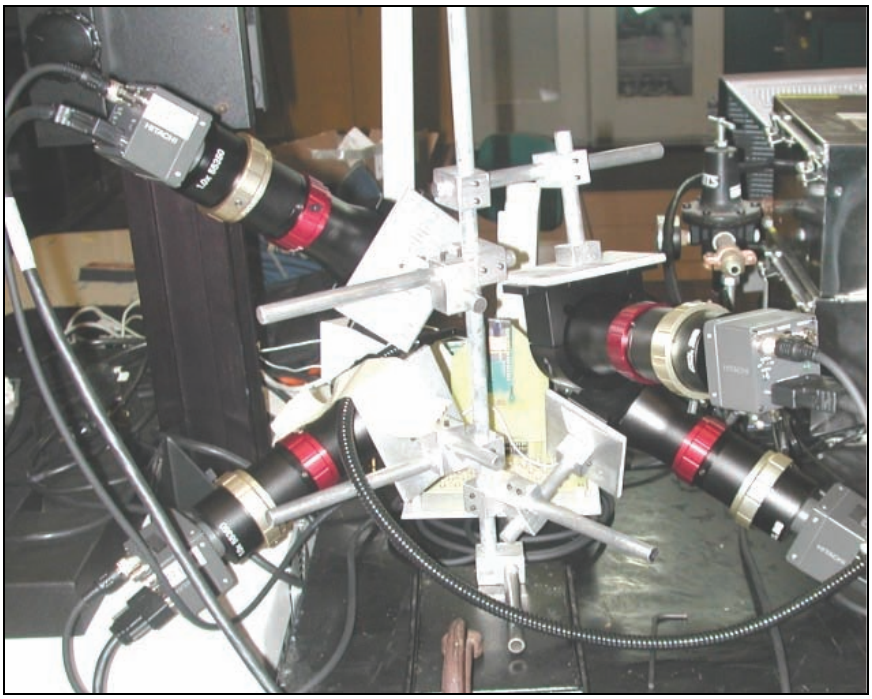

Figure 3. Four-camera photogrammetry system focused on a millimeter-scale wing.

3. Results

The wings have been tested to determine the resonant frequencies and mode shapes using an LDV. These results have been compared to a finite element (FE) modal analysis. The modal analyses show that the fundamental resonant frequency exhibits an expected longitudinal flexural mode desirable as a large flapping stroke, while the second mode is torsional pitching of the wing about a longitudinal axis, as can be seen in figure 4. These are the two most fundamental motions characteristic of insect wing kinematics, a flapping motion to move the wing relative to the air and a pitching motion to set the appropriate angle of attack to generate lift. These motions occur at the same frequency with a precisely controlled phasing in insects, which will require further refinement of the device designs to achieve with the current actuation mechanism.

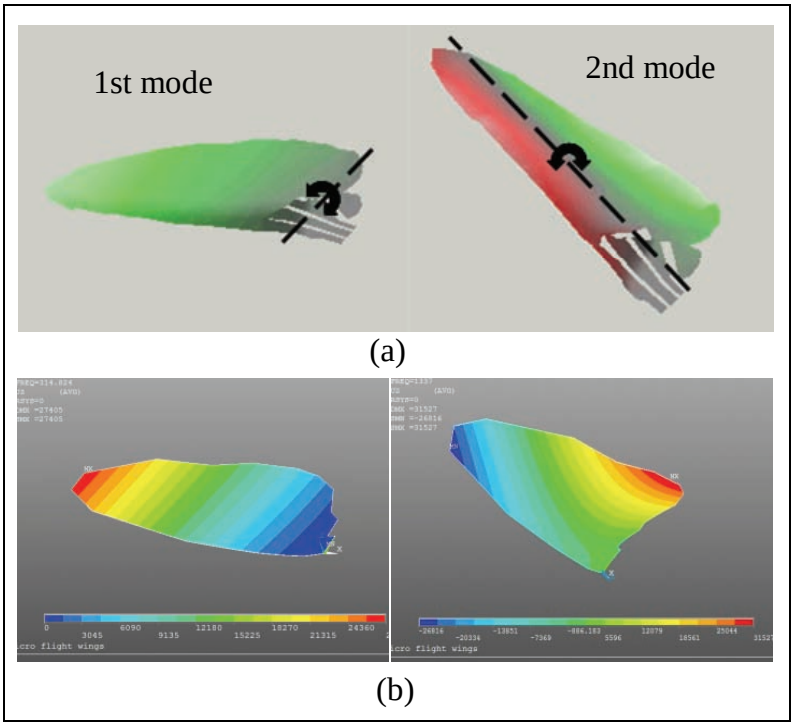

Figure 4. First two resonant mode shapes of the PiezoMEMS micro-wing (a) measured with an LDV and (b) FE model.

The fundamental resonance frequencies for a set of devices are illustrated graphically, along with one point representing the average flying Drosophila, in figure 5. As would be expected by analogy with a cantilever beam, there appears to be an inverse relationship between the span of a wing and its resonant frequency. Comparing designs of the same span, designs 1–3 vs. 4–6 (see table 1), it seems that the thickness of the elastic layer is positively correlated to the natural frequency. The elastic layer covers the entire device, actuator and wing planform. It appears

that the trend in frequency response is dominated by the stiffening effect of the thicker actuator/wing verses the softening of a higher wing mass. These basic conclusions provide some design trends but additional experiments are required to further understand how to achieve the desired kinematics.

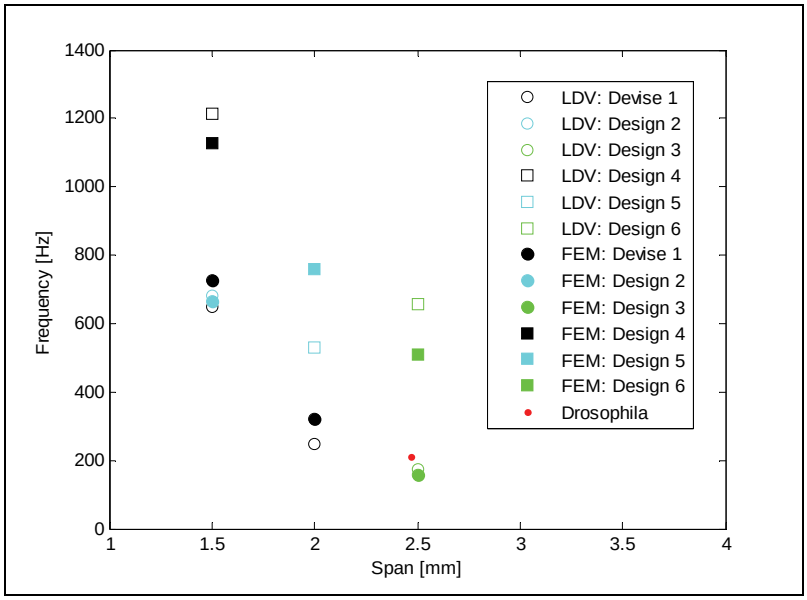

Figure 5. Fundamental resonant frequencies verses span for PiezoMEMS micro-wings.

The FE model consists of a structural model of the wing and actuators. The model is created with solid, three-dimensional, 10-node tetrahedral elements. The default element size is specified as 50 microns in length along the surface boundaries. The boundary conditions for the FE model designate that the base of the actuators are fixed in all degrees-of-freedom. The theoretical approximations do not currently account for all of the geometry, such as vein structures and residual backside Si, which contributes to the error between the theoretical and experimental results. The model also neglects aerodynamic loads, including an apparent mass term, which will contribute to a higher predicted frequency.

Inspection of long exposure optical images, as seen in figure 6, illustrates the range of wing displacement during wing flapping. The out-of-plane deformation apparent in figure 6a is a result of residual stress in the device due to fabrication. This stress will be mitigated in future designs by implementing the procedures described in reference 4. The flapping motion in figure 6b is driven by a sinusoidal 5 V peak-to-peak (p-p) excitation at the resonance frequency of 156 Hz with all three actuators in phase. The flapping motion is a result of both active bending of the piezoelectric actuators at the wing root, as well as passive deformations of the elastic wing structure due to aerodynamics and inertial forces. Depending on whether measured at the actuator or wing tip, the displacement of the wing is between 17° and 44°, respectively. As most of the aerodynamic force is produced on the outboard sections of the wing, where the speed is

the greatest, the larger value is more relevant. Although not clearly evident in the images, video of these wings makes it fairly apparent that little pitching of the wing is occurring. As noted earlier, the incorporation of this pitching motion will be a necessary condition of producing lift.

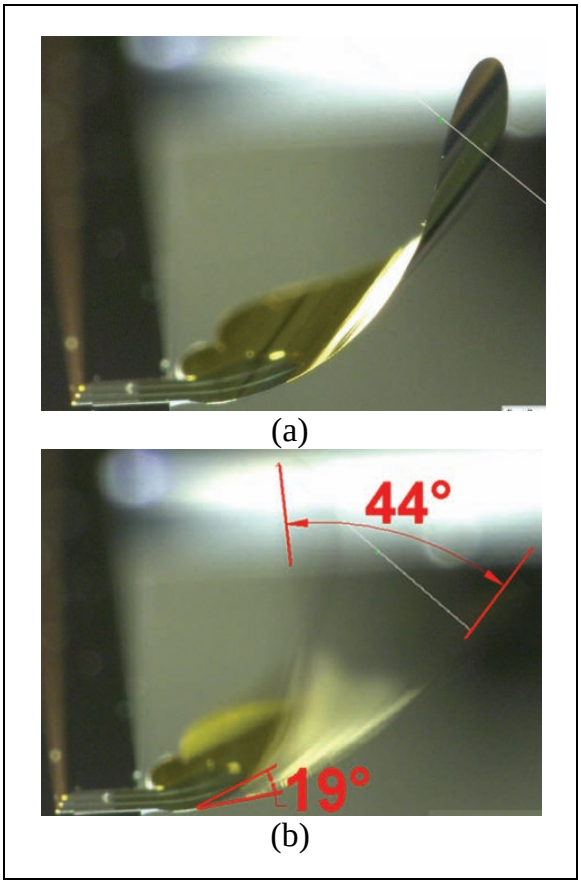

Figure 6. Images of a wing (design 3, 2.5 mm length) (a) at 0 V and (b) at resonance (156 Hz, 5 V p-p), showing that resonant behavior amplifies the stroke.

Comparison of this flapping amplitude can be made against the model Drosophila fly. The wing in figure 6 appears in figure 5 (design 3, the closest to the Drosophila data point). As can be seen in figure 5, this device of roughly the same wing span matches closely with the flapping frequency of this average Drosophila. The average flapping amplitude for the Drosophila is about 163°. As this 44° of flap amplitude is barely a quarter of that seen in Drosophila, this wing is not demonstrating the needed displacements to match this species. A larger flap amplitude may be produced with higher input voltage or a different wing composition but the most appropriate design will probably not be the same as this insect given the material difference that exist between insects and robots. There is a great diversity in the frequency, span, and amplitude across different species (5) and finding an appropriate combination to suit the constraints of MEMS fabrication seems very probable from these results.

Figure 7 illustrates the spatial location of a wing derived from images of the wing captured by the photogrammetry system. Once a series of images have been captured by the system, an optimization is performed to minimize, in a least squares sense, the difference between the identified targets in the images and the known locations of the targets on the wing. The variables optimized to minimize this difference include three coordinates and three Euler angles representing the wing position and orientation in space as well as the amplitude of several shape functions, which model out-of-plane bending and twisting. Comparisons of the distance are made between respective targets in the pixel space of the acquired images and of the targets on the three-dimensional wing transformed into each camera's image space. Target identification has proven to be difficult. Improvements to address this difficulty will address the optics and lighting of the system and the wing designs to try to reduce glare and improve image quality, as well as the implementation of a more robust algorithm for performing target identification. Once these issues have been resolved, the technique will allow the rapid collection and processing of data that can be used for parametric evaluation of the performance of various designs.

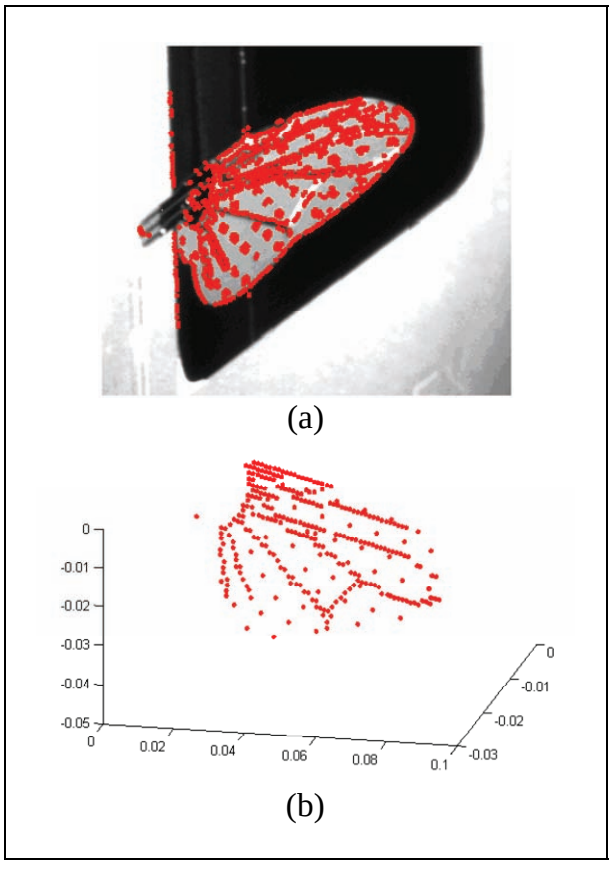

Figure 7. Wing target triangulation showing (a) an example image of the wing and identified targets and (b) the triangulated surface "veins" and targets in space.

4. Conclusions

This work reveals that it is possible to fabricate MEMS flapping-wings that can achieve stroke-amplitude and flapping frequencies similar to insects, and that this technology has great potential to produce millimeter-scale flying robots. Many additional challenges still need to be overcome before a fully operational vehicle can be produced. Solutions will be needed for full system integration of sensors, electronics, and power supply, which pose significant challenges to the long term success of these devices.

In the short term, additional characterization of the current devices is needed, including testing of the wing material properties and stiffness. Additionally, the wing design should be optimized to have structural rigidity values that more closely mimic those of insects. Another area of interest is reducing the stiffness of the wings to more closely match properties of insect wings while maintaining structural integrity and robustness. This effort has established the feasibility of achieving insect-comparable stroke amplitudes; however, force production in insects is due, in large part, to the unsteady aerodynamic effects associated with the full 3-D wing kinematics that include the angle of attack. The next step is to control the angle of attack of the wing during the wingbeat. The kinematic data will be used to calculate the aerodynamic loads produced to make determinations of the flight forces generated by the millimeter-scale wings.

5. References

1. Polcawich, R.; Pulskamp, J.; Judy, D.; Ranade, P.; Trolier-McKinstry, S.; Dubey, M. Surface Micromachined Microelectromechancial Ohmic Series Switch Using Thin-Film Piezoelectric Actuators. *IEEE Trans. Microwave Theory and Tech*. **2007**, *55*, 2642–2654.

2. Wolf, P; Dewitt, B. *Elements of Photogrammetry with Applications in GIS, 3rd Edition*, McGraw Hill Companies, Inc.: Boston, MA, 2000, 233–256.

3. Lehmann, F.; Dickinson, M. The Changes in Power Requirements and Muscle Efficiency During Elevated Force Production in the Fruit Fly Drosophila Melanogaster. *The Journal of Experimental Biology* **1997**, *200*, 1133–1143.

4. Pulskamp, J.; Wickenden, A.; Polcawich, R.; Peikarski, B.; Dubey, M.; Smith, G. Mitigation of Residual Film Stress Deformation in Multilayer Microelectromechanical Systems Cantilever Devices. *J. Vac. Sci. Technol. B* **2003**, *21*, 2482–8486.

5. Ellington, C. The Aerodynamics of Hovering Insect Flight. VI. Lift and Power Requirements. *Phil. Trans. R. Soc. London, B* **1984**, *305*, 145–181.

6. Transitions

The following two conference presentations have been accepted:

Bronson, J.; Pulskamp, J.; Polcawich, R.; Kroninger, C.; Wetzel, E. Thin Film PZT Flapping Wing Actuators for Insect-Inspired Robotics. *22nd IEEE International Conference on MEMS*, Sorrento, Italy, Jan 2009.

Kroninger, C.; Pulskamp, J.; Polcawich, R.; Bronson, J.; Wetzel, E. Design and Characterization of Millimeter-Scale Flapping Wings. *AHS International 65th Annual Forum & Technology Display*, Grapevine, TX, May 2008.

Acronyms

Al	aluminum
ARL	U.S. Army Research Laboratory
Au	gold
CCD	Charge-Coupled Device
DRIE	deep RIE
FE	finite element
LDV	laser Doppler vibrometer
MEMS	Micro-Electro-Mechanical System
Ni	nickel
PECVD	plasma enhanced chemical vapor
Pt	platinum
PZT	lead zirconate titanate
RF	radio frequency
RIE	reactive ion etch
Si	silicon
SOI	silicon-on-insulator
Ti	titanium
XeF_2	xenon difluoride

NO. OF COPIES ORGANIZATION

1 HC US ARMY RESEARCH LAB
MARK NIXON
6 EAST TAYLOR RD, MS-266
HAMPTON VA 23681-2199

1 (PDF only) DEFENSE TECHNICAL INFORMATION CTR
DTIC OCA
8725 JOHN J KINGMAN RD
STE 0944
FORT BELVOIR VA 22060-6218

1 CD DIRECTOR
US ARMY RESEARCH LAB
IMNE ALC HR
2800 POWDER MILL RD
ADELPHI MD 20783-1197

1 CD DIRECTOR
US ARMY RESEARCH LAB
AMSRD ARL CI OK TL
2800 POWDER MILL RD
ADELPHI MD 20783-1197

1 CD DIRECTOR
US ARMY RESEARCH LAB
AMSRD ARL CI OK PE
2800 POWDER MILL RD
ADELPHI MD 20783-1197

NO. OF COPIES ORGANIZATION

3 HCs DIRECTOR
8 CDs US ARMY RESEARCH LAB
AMSRD ARL SE RL
J PULSKAMP
J BRONSON
R POLCAWICH (8 CDs)
B PIEKARSKI
2800 POWDER MILL RD
ADELPHI MD 20783-1197

1 HC DIRECTOR
US ARMY RESEARCH LAB
AMSRD ARL SE R
P AMIRTHARAJ
2800 POWDER MILL RD
ADELPHI MD 20783-1197

ABERDEEN PROVING GROUND

5 HCs DIR USARL
AMSRD ARL CI OK TP (BLDG 4600)
AMSRD ARL VT UV
C KRONINGER
M BUNDY
S WILKERSON
AMSRD ARL WM MA
E WETZEL

TOTAL: 22 (1 PDF, 10 HCs, 11 CDs)

INTENTIONALLY LEFT BLANK.